

REACTIVELY SPUTTERED MoO₃ THIN FILMS AND TEMPERATURE DEPENDENCE OF ELECTRICAL PROPERTIES OF AN Ag/MoO₃/n-Si DIODE

G. CEBISLI^a, S. ASUBAY^{b,*}, Y. S. OCAK^{c,d}

^a*Department of Physics, Institute of Natural and Applied Science, Dicle University, 21280, Diyarbakir, Turkey*

^b*Department of Physics, Faculty of Science, Dicle University, 21280, Diyarbakir, Turkey*

^c*Department of Science, Faculty of Education, Dicle University, 21280, Diyarbakir, Turkey*

^d*Smart-Lab, Dicle University, 21280, Diyarbakir, Turkey*

MoO₃ thin films were deposited onto n-Si and soda lime glass substrates by the reactive sputtering method. The influence of reactive gas flows on the morphological, structural and optical properties of thin films were analyzed by Atomic Force Microscopy (AFM), X-ray Diffraction (XRD) system and UV-Vis data. It was seen that the homogeneity and amorphousness of the films increase with the O₂ ratio. In addition, the Ag/MoO₃/n-Si structure was obtained by evaporation of Ag on MoO₃/n-Si structure. It was seen that the device had excellent rectification. The electrical properties of Ag/MoO₃/n-Si structure were analyzed by current-voltage (*I-V*) measurements in the dark between 77 and 500 K. It was reported that the temperature had a strong influence on the electrical parameters of the device.

(Received September 18, 2018; Accepted November 7, 2018)

Keyword: MoO₃, Reactive sputter, Thin film, Heterojunction

1. Introduction

For a few decades, the popularity of transition metal oxide thin films have been increasing because of their usage in a wide variety of technological applications. Molybdenum oxide (MoO₃) with non-toxic and a wide band gap property is one of the most popular transition metal oxides. It has been used as large-area electrochromic devices [1], catalysts [2], solid-state microbatteries [3] and gas sensors [4]. It was shown that MoO₃ thin films have a sensitivity to NO₂, NH₃, CO and H₂ [5-7]. Recently, MoO₃ has also been highly preferred in various parts of photovoltaic devices. For instance, Liu et al. [8], demonstrated the improvement of power conversion efficiency (η) of hybrid Si/organic heterojunction solar cell from 11.1 to 13.01 % by using MoO₃ thin films as an antireflection and inversion induced layer. Moreover, MoO₃ was considered as a primary, transparent back contact in the fabrication of Cu(InGa)Se₂ based solar cells in order to use it superstrate and bifacial devices. In that study, it was proved that only 10 nm MoO₃ thin film between ITO and Cu(InGa)Se₂ thin films could improve the cell efficiency from 8 to 11.9%.

Various methods including spin coating, ultrasonic spray pyrolysis, sputtering and thermal evaporation have been chosen to deposit MoO₃ thin films [9-12]. Among all other methods, sputtering can be used to obtain homogeneous and highly controlled large area thin films of metals and ceramics. Reactive sputtering is one of the most preferred methods to deposit oxides and nitrides onto various substrates.

In this study, it was aimed to obtain MoO₃ thin films by reactive sputtering of Mo metal as target and O₂ as reactive gas, determine the influence of reactive gas flows on morphological,

* Corresponding author: sezai.asubay@gmail.com

structural and optical properties of MoO₃ thin films, use it in the fabrication of Ag/MoO₃/n-Si structure and report the temperature dependence of its electrical characteristics.

2. Experimental procedures

In the study soda lime glass (SLG) and n-type Si with (100) orientation and 1-10 \square cm resistivity were used as substrates. SLG and n-Si substrates were cleaned by RCA cleaning procedures. The native oxide layer of the n-Si wafer was removed by dipping it in diluted HF:H₂O solution for 30 s. The substrates were washed with deionized water and dried under N₂ atmosphere. Before the formation of MoO₃ thin films, an ohmic contact to n-Si was formed by evaporating of Au metal on the unpolished side of it and annealing them at 420 °C for 3 min in a quartz tube furnace flowing N₂ gas. The wafer was cut into several parts. For sputtering procedures, high purity Mo target and high purity O₂ and Ar gases were used. The MoO₃ thin films were deposited onto previously cleaned n-Si and soda lime glass substrates. The pressure of the vacuum chamber firstly was decreased to 10⁻⁶ Torr. The plasma occurred at 20 mTorr. The MoO₃ thin films were deposited at 10 mTorr pressure. The ratio of O₂/(Ar+O₂) was fixed 10, 25 and 50 % for each sputtering processes and these MoO₃ thin films were called M1, M2, and M3, respectively. The substrate temperature and the power applied to Mo target were fixed to room temperature and 100 W, respectively. The sputtering procedures continued for 15 min. The obtained thin films were annealed at 500 °C for 45 min to improve the quality of the films. The morphological, structural and optical properties of the MoO₃ thin film were determined using Park System XE-100 atomic force Microscopy (AFM), PanAnalytical X-ray Diffraction system (XRD) and Perkin Elmer Lamda 25 UV-Vis spectrometer. Ag metal was evaporated as a front contact for the MoO₃/n-Si structure obtained by sputtering during 50% O₂ flows. Electrical properties of Ag/MoO₃/n-Si structures were analyzed using Keithley 2400 sourcemeter in the dark between 77 and 500 K by the help of Janis VPF-100 Cryostats with Lake Shore 335 temperature controller.

3. Results and discussion

3.1 Determination of morphological, optical and structural properties of MoO₃ thin films

In order to see the influence of the ratio of reactive gas to Argon (O₂:Ar) on surface morphologies, the atomic force microscopy of the reactively sputtered MoO₃ thin films was carried out in non-contact mode. The 3D AFM images of the thin films are presented in Fig.1. The root mean square (RMS) of the roughness values were measured as 73.401, 19.177 and 1.119 nm for the films deposited at 10, 25 and 50 % oxygen ambient and annealed at 500 °C, respectively. The decrease in RMS values of the MoO₃ thin films with the increase in oxygen ratio directly shows the increase inhomogeneity of the film. It can be said that the low oxygen content in the films is fulfilled by annealing and the oxygen content in the structures is increased as the oxygen is used in the high concentration during the deposition process. Thus the less oxygen is injected into the structures during annealing procedures. In other words, the oxygen deficiency in the structures obtained at lower oxygen ratios is removed by annealing, and it caused deformations on the surfaces. Similarly, Gao et al.[13] deposited HfO₂ thin films in various O₂/Ar ratios. They kept Ar flow at 20 sccm and changed O₂ flow rate 0 to 16 sccm. They reported the RMS roughness of the HfO₂ thin films between 3.39 and 1.42 nm with the increase in O₂ partial pressure. Therefore, it can be said that the partial pressure of O₂ during reactive sputtering of metals have great influence on the morphological properties of oxide films.

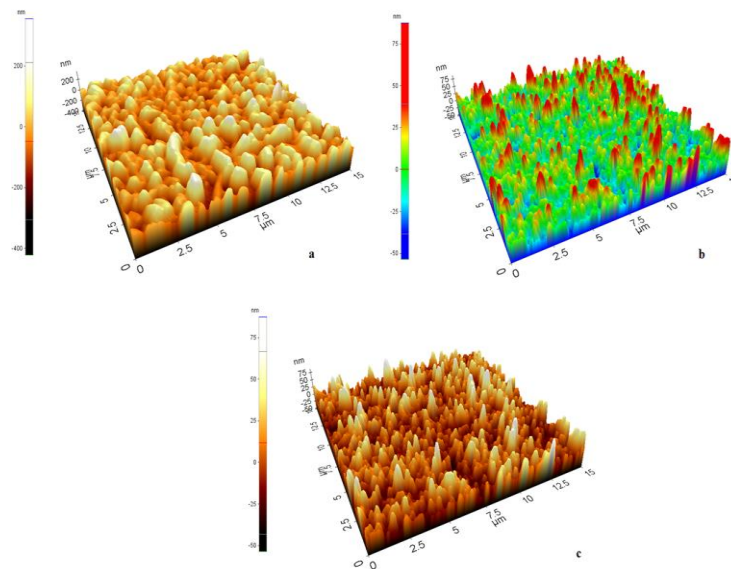


Fig. 1. 3D AFM images of reactive sputtered MoO_3 thin films deposited at a) 10 b) 25 and c) 50 % $\text{O}_2:\text{Ar}$ flows.

The absorbance vs. wavelength plots of the MoO_3 thin films deposited at 10, 25 and 50 % oxygen ambient and annealed at 500°C were presented in Fig. 2. Their absorbance vs. wavelength plots before annealing is given in supplementary materials (S1). As seen from the figures, after annealing procedures the absorption edge shift to the ultraviolet region from visible region. Additionally, it is seen that the films become more transparent with the increase in the amount of oxygen during sputtering procedures. The higher absorption values of the films before the annealing procedure refers to oxygen deficiency in the films. The band gaps of the films were calculated by means of the equation

$$\alpha h\nu = A(h\nu - E_g)^m \quad (1)$$

where α is the absorption coefficient, $h\nu$ is the energy, A is a constant, E_g is the band gap of the material and m is a constant which is $\frac{1}{2}$ for a direct band gap materials. The $(\text{Ah}\nu)^2$ -energy plots of after annealing procedures are inserted in Fig. 2. The band gaps of the films were executed from

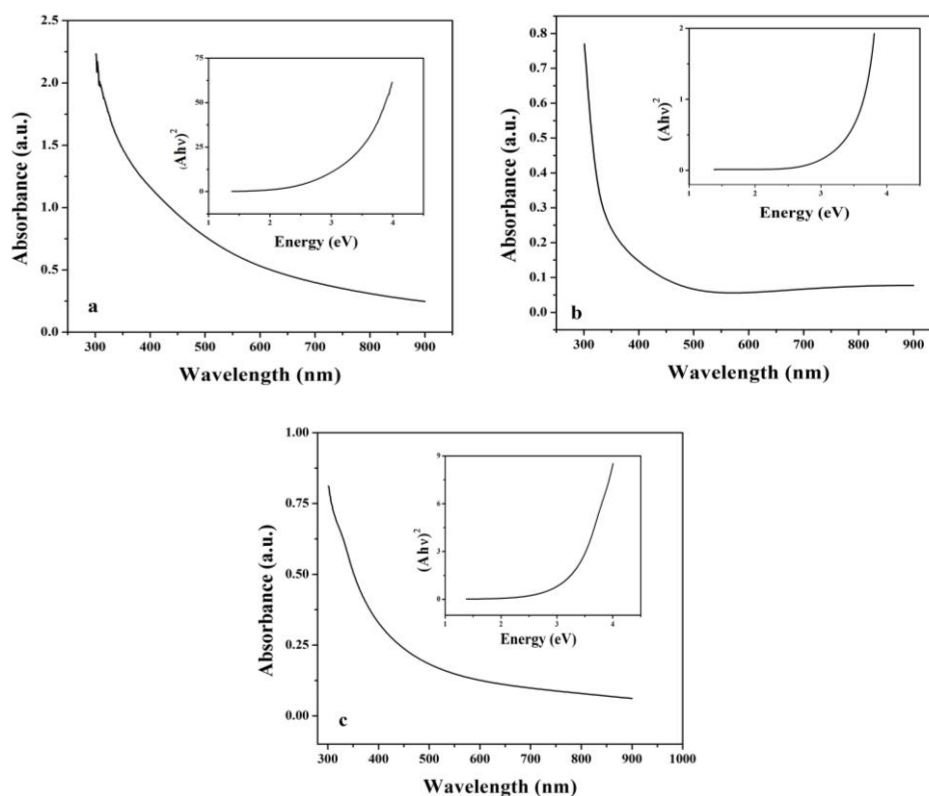


Fig. 2. The absorbance vs. wavelength and $(Ah\nu)^2$ -energy plots of the MoO_3 thin films deposited at a) 10 b) 25 and c) 50 % O_2 :Ar flows and annealed at 500 °C.

the intercepts of the plots on energy axis. The calculated band gap values are given in Table 1. As seen from the table, the band gap values of the films after annealing are higher than the ones before annealing. It implies Mo excess in the structures before annealing. The increase of the band gap with the increase of O_2 ratio during the sputtering process shows the increase of oxygen amount in the structures. The results verify the variation of RMS obtained from AFM images for the films.

Table 1. The calculated band gap values of reactively sputtered MoO_3 thin films before and after annealing.

Sample	Band Gap (eV)	Sample	Band Gap (eV)
M1 before annealing	2.82	M1 after annealing	3.24
M2 before annealing	3.11	M2 after annealing	3.30
M3 before annealing	3.28	M3 after annealing	3.29

To understand the influence of oxygen ratio on structural properties of the film the XRD patterns of the MoO_3 thin films are presented in Fig. 3. The crystal size of thin films was calculated using Scherrer's relation

$$D=0.9\lambda/\beta\cos\theta \quad (2)$$

where D is the diameter of the crystallites, λ is the wavelength of Cu- K_α radiation, β is the FWHM value of XRD peaks. The 2Θ degrees of the main peaks, full width at half maximum (FWHM) values, interplanar spacing distances and the crystal size of these peaks are presented in Table 2.

As seen from the table, the highest crystallinity of the films is observed for the film obtained at 25 % ratio, and the lowest crystallinity of the films is reported for the film obtained at 50 % ratio.

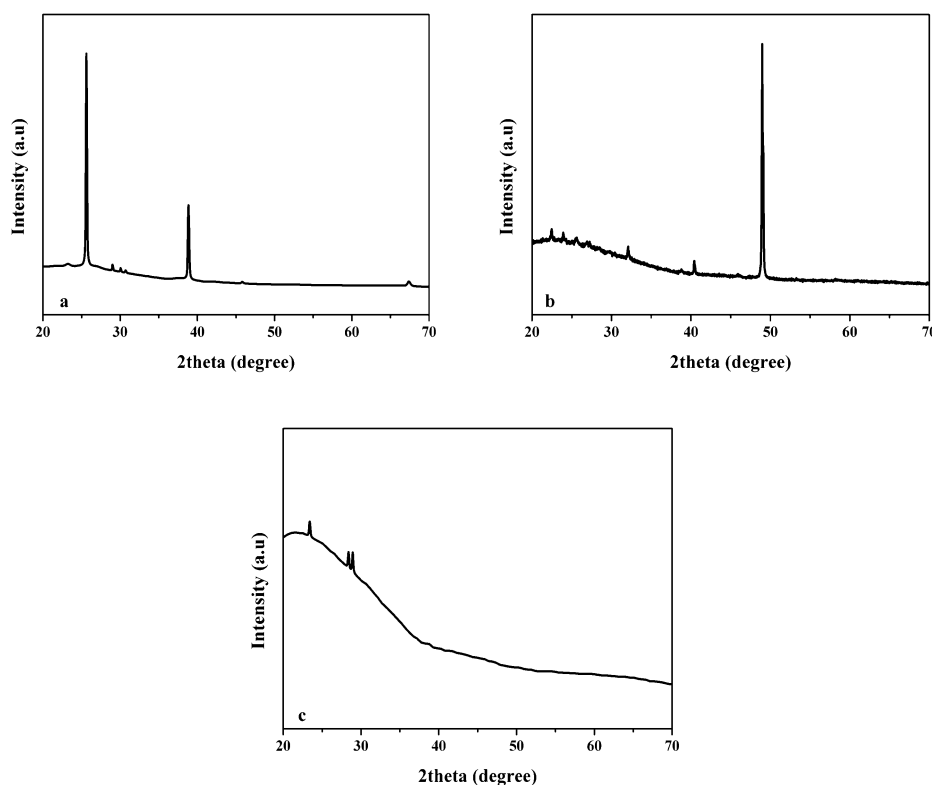


Fig. 3. XRD patterns of the MoO₃ thin films deposited at a) 10 b) 25 and c) 50 % O₂:Ar flows and annealed at 500 °C.

The MoO₃ film deposited at 1:1 (O₂:Ar) ratio has the lowest roughness value and the lowest crystal size. It implies the lower crystallinity of MoO₃ thin films for the higher O₂ ratio. Additionally, for the films growth at 10% O₂ ratio has main peaks 25.61, 29.00, 38.83 and 67.34 which are related to (040), (300), (060) and (0100) orientations. The (0k0) reflections show the orthorhombic α -phase of MoO₃[14]. For the films growth at 25 % O₂ ratio has a main peak at 49.11 related to (002) orientation and other peaks related to (110), (040), (021), (111) and (060) orientations [14, 15]. Finally, the film obtained at the highest O₂ ratio has (110), (021) and (300) reflections [15]. Therefore, it can be said that the O₂ ratio during reactive sputtering has a great influence on the structural and morphological properties of the films.

Table 2. Main XRD characteristics of MoO₃ thin films.

Sample	2 Θ	FWHM	d-spacing (Å)	Crystal Size (nm)
	(degree)	(degree)		
MoO ₃ obtained at 10 % O ₂	25.61	0.1407	34.786	62.61
	29.00	0.1023	30.786	88.80
	38.83	0.1535	23.195	66.43
	67.34	0.3582	13.905	57.57
MoO ₃ obtained at 25 % O ₂	23.93	0.1535	37.194	56.62
	25.59	0.2558	34.814	34.43
	26.86	0.6140	33.193	14.50
	32.08	0.1023	27.901	91.65
	38.78	0.6140	23.220	165.98
	49.11	0.0936	18.582	129.66
MoO ₃ obtained at 50 % O ₂	23.39	0.1791	38.039	48.33
	28.37	0.1535	31.460	58.82
	28.91	0.1535	30.884	59.12

3.2 The temperature-dependent current-voltage behavior of an Ag/MoO₃/n-Si structure

Ag/MoO₃/n-Si device was fabricated by evaporation of Ag metal onto MoO₃/n-Si structure obtained by deposition of MoO₃ at O₂:Ar (1:1) atmosphere. It was seen that the Ag/MoO₃/n-Si structure had an excellent rectification at room temperature. To see the influence of temperature on current-voltage (*I-V*) characteristics of the diode, *I-V* measurements were carried out between 77 and 500 K. Fig.4 demonstrates the semi-logarithmic *I-V* plots of Ag/MoO₃/n-Si in the given range. As seen from the figure, the temperature has a strong influence on the *I-V* characteristics of the device. The reverse bias current, especially, increases rapidly with the increase of temperature. The relationship between applied voltage (*V*) and current (*I*) of a diode with series resistance can be expressed as [16]

$$I = I_0 \exp\left(\frac{q(V - IR_S)}{nkT}\right) \quad (3)$$

where I_0 is the saturation current, q is the electronic charge, R_S is the series resistance, n is the ideality factor, k is the Boltzmann constant and T is the absolute temperature. The I_0 saturation current can be written as

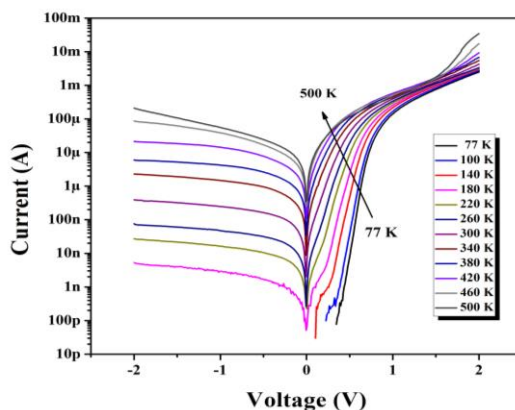


Fig. 4. Semi-logarithmic I-V plots of Ag/MoO₃/n-Si between 77 and 500 K.

$$I_0 = SA^*T^2 \exp\left(-\frac{q\phi_b}{kT}\right) \quad (4)$$

where S is the diode area ($S = 0.0176174 \text{ cm}^2$), A^* is Richardson constant and ϕ_b is the barrier height. The ideality factor values of the Ag/MoO₃/p-Si diode were calculated using the slope values of $\ln I$ - V plots with the help of the equation

$$n = \frac{q}{kT} \frac{dV}{d \ln(I)} \quad (5)$$

The main electrical parameters of the diode calculated between 77 and 500 K are given in Table 3. As seen from the table, the diode has an ideality factor value as 2.282 for 300 K. It should be unity in an ideal case. But the deviation from unity implies the influence of the series resistance of the device or inhomogeneity at the interface. The ideality factor vs. temperature plot is presented in Fig. 5. As seen from Fig. 5 and Table 3, the ideality factor values decreased from 4.391 to 1.627 with the increase in temperature. The barrier heights of the Ag/MoO₃/p-Si diode were executed using both saturation current values and the equation 4. The barrier height vs. temperature plot of the diode is also demonstrated in Fig. 5. It can be seen from both Table 3 and Fig. 5 that the barrier height values of the diode increase linearly with temperature from 0.307 eV (77 K) to 1.131 eV (500 K). The increase in barrier height and the decrease in ideality factor values with temperature have been reported for similar structures [17-19].

For instance, Ocak et al. [18] fabricated Al/MoS₂/n-Si heterojunction by sputtering of a MoS₂ target onto the n-Si semiconductor and determined its electrical parameters between 150 and 400 K. They have reported that while ideality factor decreased from 2.304 (150 K) to 1.020 (400 K), the barrier height increased from 0.419 (150 K) to 0.867 eV (400 K).

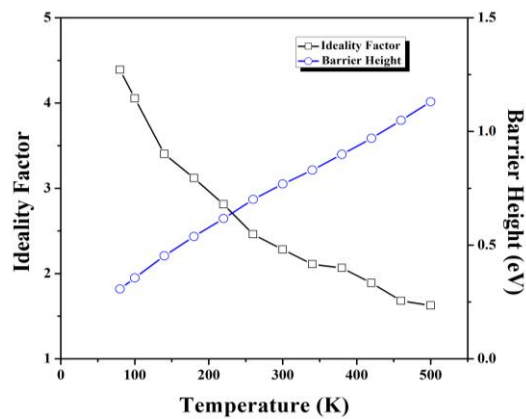


Fig. 5. The dependence of both ideality factor and barrier height to temperature for Ag/MoO₃/n-Si diode.

The deviation from linearity in forward bias I - V plots of the diode is because of the influence of the series resistance caused by the contact points or bulk resistance of the MoO₃ thin film. The series resistance of the diode can be analyzed using the method proposed by Norde. He defined a function written as [20]

$$F(V) = \frac{V}{\gamma} - \frac{kT}{q} \left(\frac{I(V)}{SA^*T^2} \right) \quad (6)$$

where γ is the first integer greater than ideality factor and $I(V)$ is the current executed from current-voltage measurements. Fig. 6 presents the $F(V)$ - V plots of Ag/MoO₃/n-Si rectifying device between 77 and 500 K. To calculate barrier height values of the structure, the minimum values of each $F(V)$ vs. V plot should be determined. The barrier heights can be determined through the relation

Table 3. Electrical parameters of Ag/MoO₃/n-Si diode between 77 and 500 K.

	lnI-V		Norde	
	n	ϕ_b (eV)	ϕ_b (eV)	R_s (Ω)
77	4.392	0.307	0.409	2668
100	4.055	0.356	0.444	2317
140	3.402	0.453	0.561	2246
180	3.120	0.538	0.623	2163
220	2.813	0.617	0.719	2094
260	2.460	0.701	0.784	1867
300	2.282	0.769	0.827	1599
340	2.109	0.830	0.867	1493
380	2.066	0.899	0.925	1391
420	1.889	0.970	0.987	938
460	1.680	1.049	1.043	681
500	1.627	1.131	1.124	378

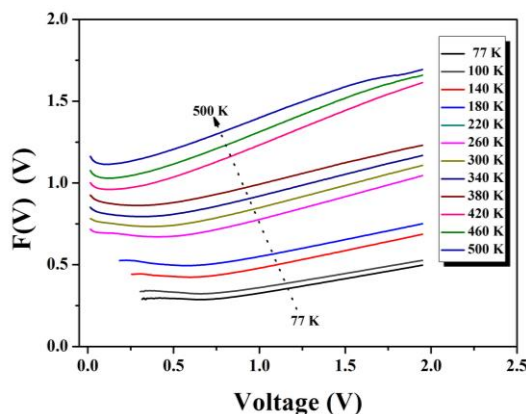


Fig. 6. Norde plots of Ag/MoO₃/n-Si rectifying device

$$\varphi_b = F(V_0) + \frac{V_0}{\gamma} - \frac{kT}{q} \quad (7)$$

where the $F(V_0)$ and V_0 are defined as the minimum of Norde function and corresponding voltage values. Additionally, the series resistance values of the diode are defined using the equation [20]

$$R_s = \frac{kT(\gamma - n)}{qI_{min}} \quad (8)$$

where I_{min} the corresponding current value at V_0 . Both barrier height and series resistance values of the structure for each temperature are also submitted in Table 3. As seen from Table 3 and Fig.7, series resistance the device decreased from 2668 to 378 Ω with the temperature. Furthermore, the barrier height obtained using Norde functions are between 0.409 (at 77 K) and 1.124 eV (at 500 K). While only linear region of $\ln I$ -V plot taken for the calculation of barrier height values in $\ln I$ -V method, whole forward bias region is taken into account in Norde method. Therefore, the variations in barrier height values calculated using $\ln(I$ -V) and $F(V)$ -V plots can be attributed to the differentiation of the methods.

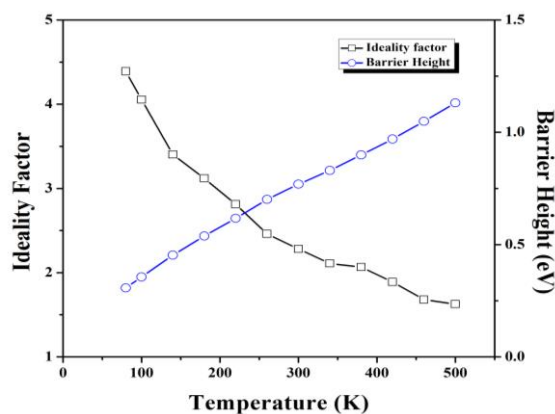


Fig. 7. Barrier height and series resistance values of Ag/MoO₃/n-Si rectifying device obtained by Norde Functions

4. Conclusions

MoO₃ thin films were deposited by reactive sputtering of Mo in various O₂ flows. Other parameters including substrate temperature, applied voltage and deposition time were fixed during

the sputtering procedures. It was seen the O₂ ratio had strong effects on structural, morphological and optical properties of the films. An Ag/MoO₃/n-Si diode was obtained by evaporating Ag metal on MoO₃/n-Si surface. The temperature dependence of electrical parameters of the Ag/MoO₃/n-Si diode was analyzed using current-voltage measurements between 77 and 500 K.

Acknowledgments

This study is supported by DUBAP with 15-ZEF-07 grand number

References

- [1] W. Dong, Y. Ly, L. Xiao, Y. Fan, N. Zhang, X. Liu, *ACS Applied Materials & Interfaces* **8**(49), 33842 (2016).
- [2] Y. Shen, X. Lu, X. Ma, J. He, D. Zhang, H. Zhan, Q. Xia *Kinetics and Catalysis* **58**(1), 28 (2017).
- [3] C. Chen, R. A. Eichel, P. H. L. Notten, *Journal of Electroceramics* **38**(2-4), 230 (2017).
- [4] W. S. Kim, H. C. Kim, S. H. Hong *Journal of Nanoparticle Research* **12**(5), 1889 (2010)
- [5] A. K. Prasad, D. J. Kubinski, P. I. Gouma, *Sensors and Actuators B: Chemical* **93**(1), 25 (2003).
- [6] E. Comini, L. Yubao, Y. Brando, G. Sberveglieri, *Chemical Physics Letters* **407**(4), 368 (2005).
- [7] C. Imawan, H. Steffes, F. Solzbacher. *Sensors and Actuators B: Chemical* **77**(1), 346 (2001).
- [8] R. Liu, S. T. Lee, B. Sun, *Advanced Materials* **26**(34), 6007 (2014).
- [9] C. Giroto, E. Voroshazi, D. Cheyns, P. Heremans, B. P. Rand, *Applied Materials & Interfaces* **3**(9), 3244 (2011).
- [10] H. H. Afify, S. A. Hassan, A. Abouelsayed, S. E. Demian, H. A. Zayed, *Thin Solid Films* **623**, 40 (2017)
- [11] V. Nirupama, S. Uthanna, *Journal of Materials Science: Materials in Electronics* **27**(4), 3668 (2016).
- [12] L. Barkat, M. Hssein, Z. El Jouad, L. Cattin, G. Louarn, N. Stephant, A. Khelil, M. Ghamnia, M. Addou, M. Morsli, J. C. Bernède, *Physica Status Solidi (a)*, **214**(1), 1600433 (2017).
- [13] J. Gao, G. He, B. Deng, D. Q. Xiao, M. Liu, P. Jin, C. Y. Zheng, Z. Q. Sun, *Journal of Alloys and Compounds* **662**, 339 (2016).
- [14] A. Hojabri, F. Hajakbari, A. E. Meibodi, *Journal of Theoretical and Applied Physics* **9**(1), 67 (2015).
- [15] K. Khojier, H. Savaloni, S. Zolghadr, *Applied Surface Science* **320** (Supplement C), 315 (2014)
- [16] E. H. Rhoderick, E. Rhoderick, *Metal-Semiconductor Contacts*, 1978, Clarendon Press Oxford.
- [17] O. Metin, S. Aydogan, K. Meral, *Journal of Alloys and Compounds* **585**, 681 (2014)
- [18] Y. S. Ocak, C. Bozkaplan, H. S. Ahmed, A. Tombak, M. F. Genisel, S. Asubay, *Optik-International Journal for Light and Electron Optics* **142**, 644 (2017).
- [19] M. L. Grilli, S. Aydogan, M. Yilmaz, *Superlattices and Microstructures* **100**, 924 (2016).
- [20] H. Norde, *Journal of Applied Physics* **50**(7). 5052 (1979).